Proceedings of ASME Turbo Expo 2011
GT2011
June 6-10, 2011, Vancouver, British Columbia, Canada

GT2011-45425

THREE DIMENSIONAL DESIGN AND OPTIMIZATION OF A TRANSONIC ROTOR IN AXIAL FLOW COMPRESSORS

Hidetaka Okui
Mitsubishi Heavy Industries, LTD
2-2-1 Shinhama Arai-Cho Takasago,
Hyogo 676-8686 Japan
Email: hidetaka_okui@mhi.co.jp

Tom Verstraete, R.A.Van den Braembussche, Zuheyr Alsalihi
von Karman Institute for Fluid Dynamics
Turbomachinery and Propulsion Department
Waterloose steenweg 72, 1640 Sint-Genesius-Rode, Belgium
Email: tom.verstraete@vki.ac.be, vdb@vki.ac.be, alsalihi@vki.ac.be

ABSTRACT

This paper presents a 3-D optimization of a moderately loaded transonic compressor rotor by means of a multi-objective optimization system. The latter makes use of a Differential Evolutionary Algorithm in combination with an Artificial Neural Network and a 3D Navier-Stokes solver. Operating it on a cluster of 30 processors enabled the optimization of a large design space composed of the tip camber line and spanwise distribution of sweep and chord length. Objectives were an increase of efficiency at unchanged stall margin by controlling the shock waves and off-design performance curve.

First, tests on a single blade row allowed a better understanding of the impact of the different design parameters. Forward sweep with unchanged camber improved the peak efficiency by only 0.3% with a small increase of the stall margin. Backward sweep with an optimized S shaped camber line improved the efficiency by 0.6% with unchanged stall margin. It is explained how the camber line control could introduce the forward sweep effect and compensate the negative effects of the backward sweep.

The best results (0.7% increase in efficiency and unchanged stall margin) have been obtained by a stage optimization that also considered the spanwise redistribution of the rotor flow and loading to reduce the Mach number at the stator hub.

INTRODUCTION

The recent trend to increase the capacity of modern heavy duty gas turbine compressors requires high performance transonic rotors with increasing tip Mach numbers. It is well known that the highly three-dimensional flow in those rotors, is associated with a radially swept shock wave [1,2]. New sophisticated design approaches based on 3-D CFD and rig tests are therefore needed to maximize their performance.

Blade sweep is known to be an effective technique to redistribute the radial loading [3,4] and has been widely used to control the shock wave in transonic fans and rotors. Backward sweep was initially investigated by Wennerstrom et al [2]. They developed a three-dimensional shock structure model and built an aft-swept blade, rotor6, to strengthen the sweep effect. This rotor showed a significant improvement of the peak efficiency [5,6] but a large decrease of the stall margin.

After several investigations, Wadia et al [7] concluded that the penalty on the stall margin was caused by the locally high loading at the tip section resulting in a stronger bow shock and an accumulation of the low momentum fluid at the tip section. In addition, no efficiency gain was achieved with the aft-swept blade in spite of the better performance of the inboard section. On the contrary, forward sweep demonstrated a significant improvement in stall margin and a slightly higher peak efficiency.

Shock waves tend to be normal to the casing wall and in combination with the forward sweep become oblique in the blade to blade surface. This reduces the losses and stabilizes the blade flow. The result of the numerical investigations of Xu and Denton [8] and Blaha et al [9] supported this conclusion about the advantage of forward sweep, but opposite results are also reported [10].

Ji [11] reviewed the previous studies in 2005, and concluded that sweep is a Degree Of Freedom (DOF) that controls the spanwise matching between the blade to blade flows. It is therefore incomplete to discuss the performance and stability according to the type of sweep only. The impact of sweep depends also on the original loading distribution, which is affected by other design parameters. Several researchers indicated that the thickness distribution [6], camber distribution [12] and solidity [13] have an equally large influence on the performance of transonic rotors as sweep and that they need to be optimized simultaneously.

Another aspect of sweep is that it often disturbs the matching with the following stage due to a radial redistribution of the loading [7,9].

Watanabe and Zangeneh [14] used an inverse method to design a swept transonic fan aiming to compensate the change in specific work and pressure ratio caused by the given forward sweep. They reasonably recovered the speed line and achieved an efficiency improvement of 0.5% by specifying a very smooth loading distribution at the tip. The method, however, did not include the tip clearance flow and the sweep was not optimized for the given loading distribution but explicitly specified.

Inverse methods seem to be suited for the design of transonic fans and rotors, since the loading or pressure distribution can be explicitly specified and the geometry, which satisfies the given design intend almost exactly, is quickly found [15]. However, it experiences some practical difficulties in establishing the design criteria for the loading distribution and in imposing the mechanical constraints.

In this study, an efficient optimizing design system developed at the von Karman Institute [16,17] has been applied to a moderately loaded transonic rotor corresponding to heavy-duty gas turbine compressors. A multi-objective optimization for the design and off-design operation was carried out, in which the sweep, chord length and the camber distributions are controlled. By tailoring these parameters simultaneously, the global loading distribution was optimized so that the stability and the performance are improved. A constant speed line calculation evaluated the off-design performance.

Three studies have been carried out. The sweep and the chord length were optimized in the first one. The camber distribution was added as an additional variable in the second one. The purpose of these cases was to validate the design method and to clarify the effect of the camber line control. Finally, a stage optimization was made to see the possible impact of previous design parameters on the stage performance.

BASELINE BLADE GEOMETRY

The specification of the original blade design is summarized in table 1. The new blade that was designed for this study is a typical front stage transonic rotor for heavy duty gas turbines. The baseline blade geometry was defined by Multiple Circular Arcs (MCA) at 5 representative sections (10, 30, 50, 70, and 90% span). The other sections were obtained by interpolation in the radial direction. No lean or sweep was introduced yet. The Controlled Diffusion Airfoil (CDA) design concept was applied to the entire span and the shock wave was appropriately controlled at the tip section so that it attached to the leading edge at the design point. As a result, the adiabatic efficiency of this baseline rotor, predicted by CFD, was already high. To achieve a further efficiency gain by optimization was therefore a quite challenging task.

Table1 Specification of the baseline blade design

Pressure ratio	1.35	-
Specific flow	180.6	kg/s/m^2
Number of blades	22	
Corrected speed	3600	rpm
Tip relative Mach number	1.20	-
Mid Diffusion Factor	0.34	-
Tip clearance	0.3	%height

OPTIMIZATION METHOD

Figure 1 shows the algorithm of the optimization system used for the present study. One of its advantages is the use of a metamodel based on an Artificial Neural Network (ANN) as an interpolation tool by which the performance corresponding to the given design parameters are predicted. It reduces the large computational cost of evaluating the blade performance by 3D-CFD and, consequently, enables an increase of the number of DOF for the optimization. These advantages have been demonstrated by many complicated 3D industrial design problems [18-21].

The algorithm consists of 2 steps. The first one is an approximated loop with ANN predictions based on the information stored in the database. The Differential Evolutionary (DE) algorithm selects promising designs that are verified in an accurate loop by means of a full 3D Navier-Stokes solver. The results of these evaluations are added to the database which allows improvements to the accuracy of the next ANN predictions. This cycle is repeated until the CFD confirms that the design requirements are achieved. A more detailed description is given in [16] and [17]. The following subsections summarize some components and their application.

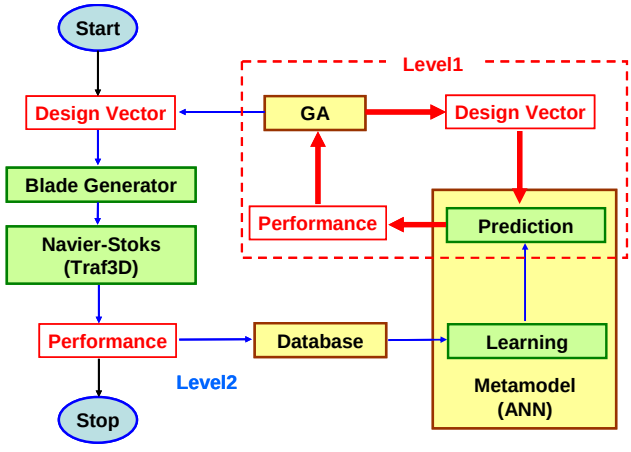

Fig.1 Optimization Algorithm

Navier-Stokes evaluation

The performance of new blades was evaluated by means of the Reynolds averaged full 3D Navier-Stokes solver TRAF3D, which was validated with the experimental data of Rotor67 [22]. The convection term is discretized by Jameson's central

differential scheme and stabilized by artificial dissipation. Turbulence closure is by the Baldwin-Lomax model. The boundary layer on the blade surface was assumed to be fully turbulent from the leading edge on. The accuracy was verified by comparing predictions of several similar geometries with MHI in-house data. In addition, all of the efficiency gains and the stall margin achieved in each optimization study have been confirmed by the ANSYS CFX with SST turbulence model.

The stall limit was defined as a point where the flow field becomes numerically unstable. A threshold of the residual was defined in advance, based on several numerical tests. In order to find the stall and peak efficiency point, calculations were done at 7 points on a constant speed line using 30 CPU's of the VKI parallel computing system.

Figure 2 shows the computational mesh used for the analysis. The structured H-type mesh has 220×53×53 points in the stream, pitch and spanwise directions respectively. In order to avoid the grid dependency on the shock wave, more than 100 grid lines were clustered in the front passage area where the bow shock is expected. The minimum grid spacing from the wall was adjusted to y+<5 in accordance with the requirements of the Baldwin Lomax turbulence model. The downstream grid is parallel to the expected exit flow angle to avoid artificial dissipation of the wake. The dependency of the performance on these parameters was carefully evaluated in advance by the verification tests.

The spanwise distributions of the absolute total pressure and temperature, swirl and pitch angle were specified as inlet boundary conditions. The average static pressure was imposed at the exit. The spanwise variation is obtained from radial equilibrium. A constant speed line is obtained by modifying the back pressure and leaving the inlet conditions unchanged.

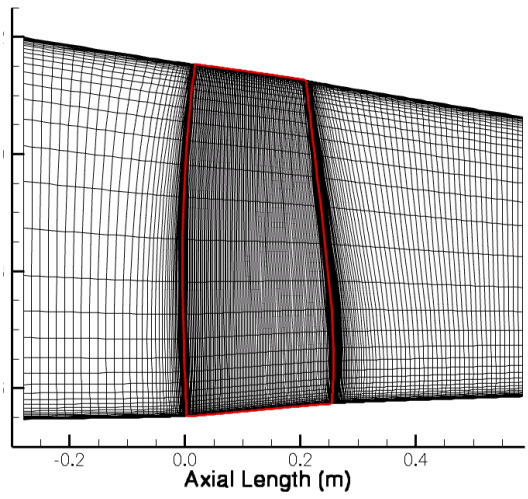

Fig.2 Computational Mesh

Geometry Definition

New blades are defined by the camber line, thickness distribution, spanwise distribution of chord length and stacking line. They are defined by B-Spline curves to create a smooth and reasonable distribution. Figure 3 explains the spanwise parameterization of the sweep and spanwise chord length. The latter are linked to each other by the spanwise positions to reduce the number variables. Sweep is defined by 6 parameters. These variables can be positive or negative corresponding to forward or backward sweep. The chord length is specified by 4 parameters as a fraction of the local chord length of the original blade.

Figure 4 shows the parameterization of the camber line. It is defined by the local slope angle which directly relates to the local loading. The current definition requires only 4 variables. The 2 additional control points are displaced together with the leading, trailing edge and the third point. They intend to keep the curvature in the front and rear parts unchanged in order to avoid undesirable local accelerations or decelerations.

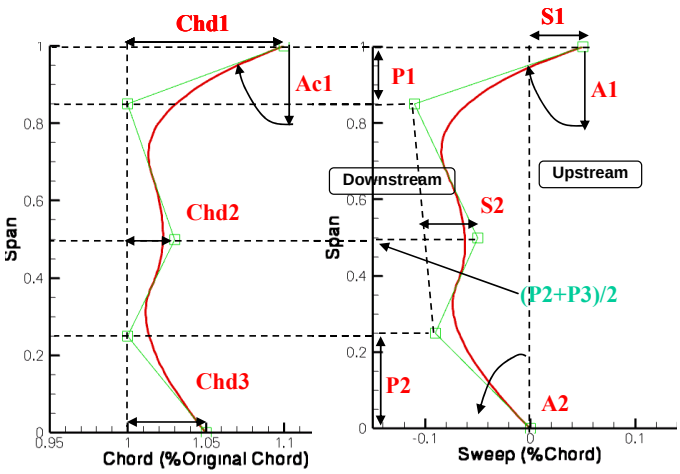

Fig.3 Parameterization of Sweep and Chord length

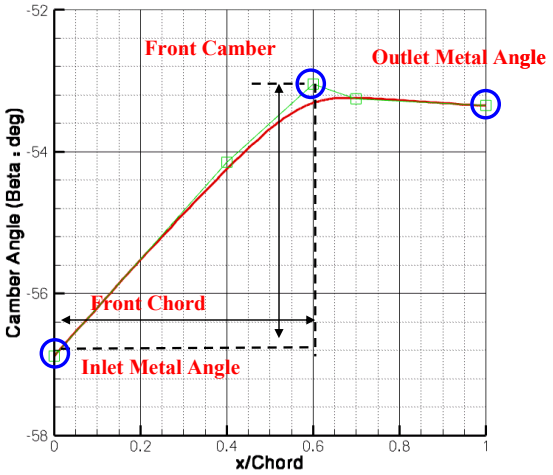

Fig.4 Parameterization of Camber-line

The main advantages of defining the camber by its slope are its relative simplicity, smoothness and the capacity to represent relatively complicated camber lines. The exit camber angle was kept constant in the single row optimizations, to guarantee the stage matching. It was a variable in the stage optimization, because the matching was then implicitly guaranteed by the stage performance.

The thickness distribution was always maintained at its original value to eliminate the effect on throat area and to avoid mechanical problems.

It was verified that this parameterization could accurately reproduce the baseline airfoil.

Problem definition

The optimization requires the transformation of the given engineering problem into a mathematical one by defining objective and constraint functions [17]. A multi-objective optimization aiming for higher performance and unchanged stability was carried out by minimizing the following objective functions.

$$\text{Obj1} = 1.0 - (\text{Peak Efficiency}) \quad (1)$$

$$\text{Obj2} = 0.3 - (\text{Throttle Margin}) \quad (2)$$

where the throttle margin is the ratio between the exit corrected mass flow at stall and the exit corrected mass flow of the baseline blade at the design point ($=m_{out\_design} / m_{out\_stall}-1$).

The optimization is governed by following constraints.

$$\text{Cons1} = (m_{in}\_choke_{baseline}) - (m_{in}\_choke_{design}) \le 0 \quad (3)$$

where m_{in} is the inlet corrected mass flow. Equation (3) requires that the choking mass flow is larger than or equal to the baseline one.

$$\text{Cons2} = (m_{out\_design} - m_{out\_stall}) \times (m_{out\_choke} - m_{out\_design}) \ge 0 \quad (4)$$

so that a new speed line includes the design throttle point.

These definitions allow a small change of the speed line resulting from the swept stacking and thus accelerate the optimization.

RESULT AND DISCUSSION

The first optimization allows only a variation of sweep and chord length. The optimized geometry is shown in Fig.5. It results from the combination of a strong forward sweep and increased chord length in the tip region. The chord length at 80% height is reduced by 5% but is almost back to its original value at the tip.

The compressor performance map is shown in Fig.6. It confirms the stability and efficiency gain attributed to forward sweep by previous researcher's [7,8]. The resulting blade achieves a reasonable improvement (0.3%) of the peak efficiency while the choking and stall margin are maintained.

A small efficiency drop is observed near stall point. It is due to a large separation in the mid span region. This inception of stall is caused by a stronger shock wave, which is associated with the increase of the local loading induced by the forward sweep. This loading shift due to the forward sweep is confirmed later in Fig.10.

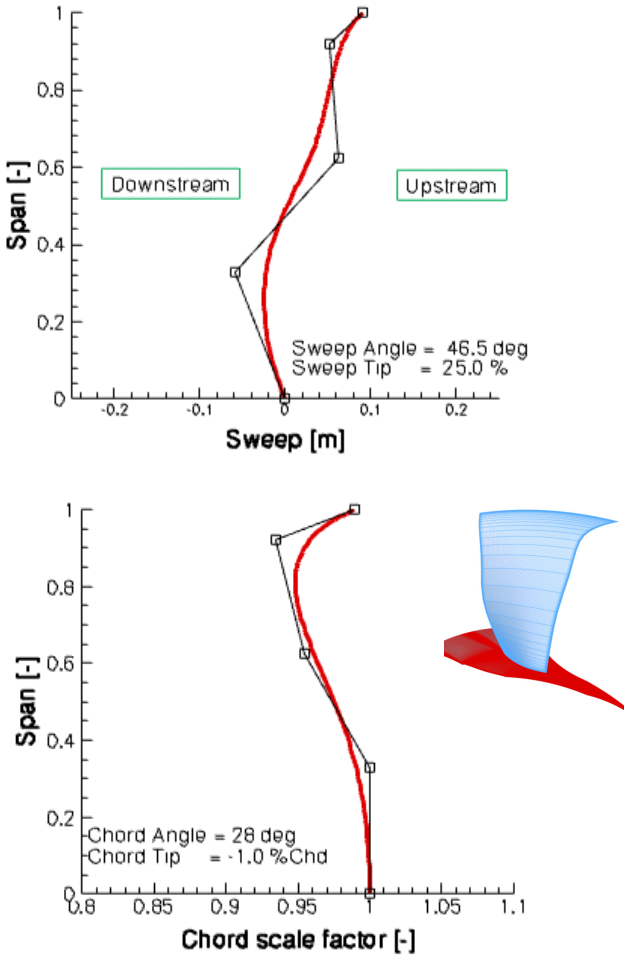

Fig.5 Resultant Geometry of the first Optimization

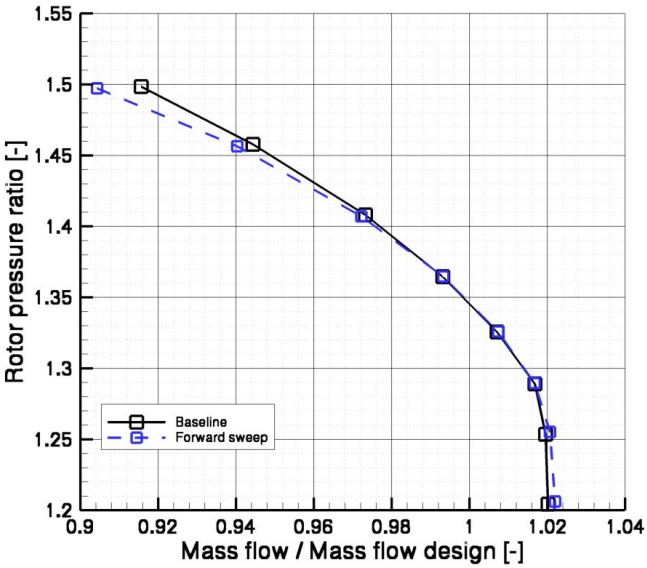

Fig.6.a Compressor map : Speed line

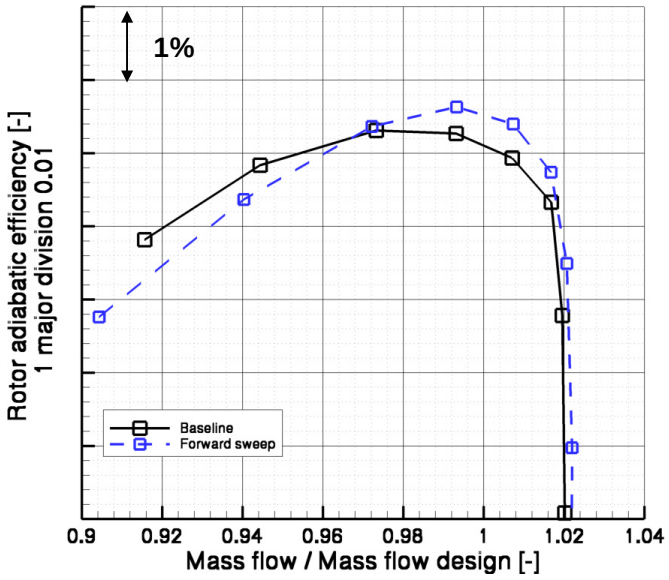

Fig.6.b Compressor map : Perfomance map

On the contrary, the tip region is quite healthy even when the flow is reduced by 10% from the choking mass flow. The resulting performance curve satisfies the design requirements specified into the objective and the constraint functions. A more detailed discussion of the flow mechanisms near stall point is out of scope of the present paper.

The Design point flow pattern is compared with the one of the baseline blade on Figs. 7 to 10. The results shown here also include those for the backward swept blade, which is the outcome of the second optimization and explained in the following subsection. The same color scales are used for each group of three figures, so that one can directly compare the strength of the shock wave, the level of the Mach number and the magnitude of the loss.

Figure 7 is the meridional view of the static pressure contours on the suction surface. Compared with the baseline blade, the passage shock became slightly weaker and the bow shock has disappeared in the tip region. The tip region is covered by the Mach cone attached at the tip leading edge as a consequence of the large sweep angle at the tip. The corresponding pressure distortion is visible upstream of the swept blade.

The static pressure contours on the blade to blade surface are shown in Fig.8. The red line on the small meridional contours at the right lower corner shows the surface of reference. Compared with the baseline blade, it is found that the new blade has a lower approaching Mach number to the leading edge on the suction side and a lower tip loading. The latter has been estimated from the pressure difference between the suction and the pressure side. Moreover, the passage flow experiences only a single passage shock since the bow shock has disappeared from the tip suction side. This reduced the local shock loss. In addition, the strong forward sweep made the bow shock bifurcated and oblique, followed by the passage normal shock, in the blade to blade surface. The flow at 70% span is almost identical to that of the baseline blade.

In order to see the effect on the tip leakage vortex, the entropy contours at the 99% height are compared in Fig.9. The high entropy region, marked by yellow and red, indicates the tip vortex. It shows that the leakage vortex is weakened and turned in the downstream direction. The vortex no longer impinges on the adjacent blade while the vortex of the baseline blade does. In the latter the low momentum fluid leaks again to the suction side of the adjacent blade. This “double leakage” [23,24] contributes also to the thicker wake of the baseline

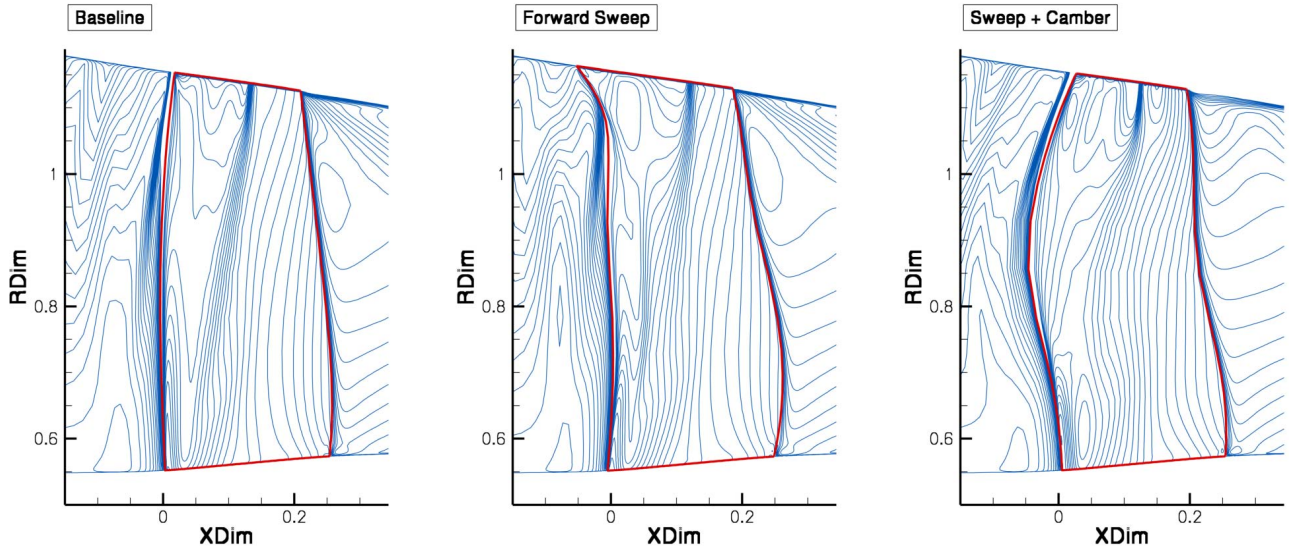

(a) Baseline Blade (b) 1st Optimization Blade (c) 2nd Optimization Blade

Fig.7 Meridional view of static pressure contour on suction surface

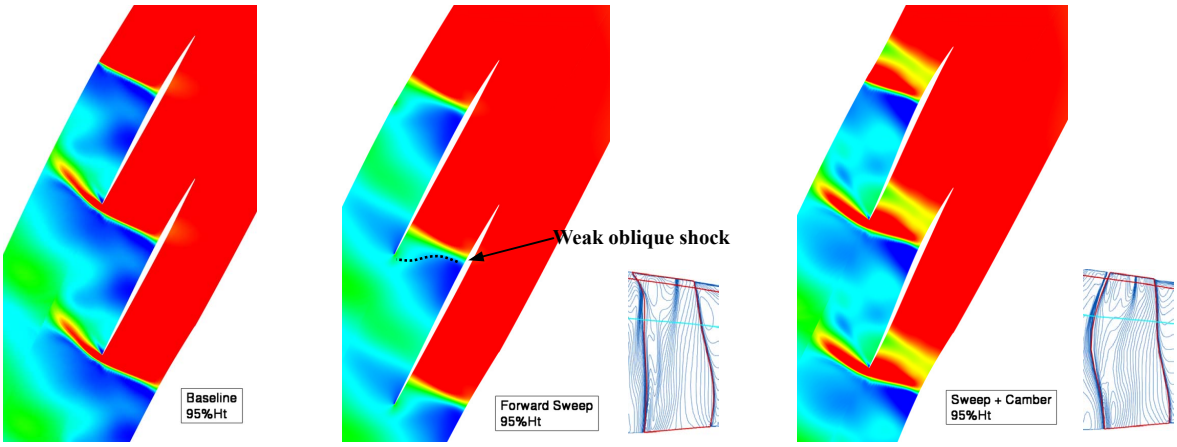

(a) Baseline Blade at 95%Ht (b) 1st Optimization Blade at 95%Ht (c) 2nd Optimization Blade at 95%Ht

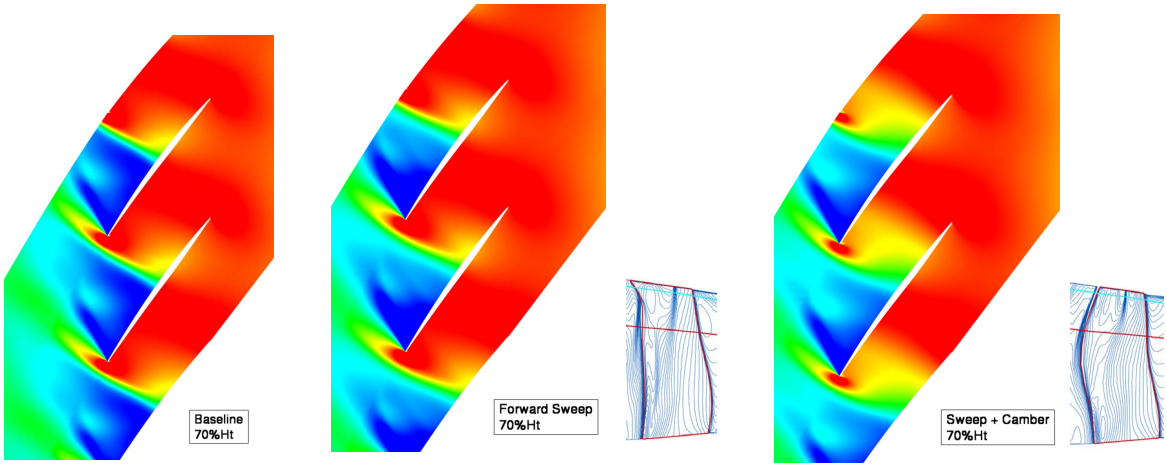

(d) Baseline Blade at 70%Ht (e) 1st Optimization Blade at 70%Ht (f) 2nd Optimization Blade at 70%Ht

Fig.8 Static pressure contour on blade to blade surface

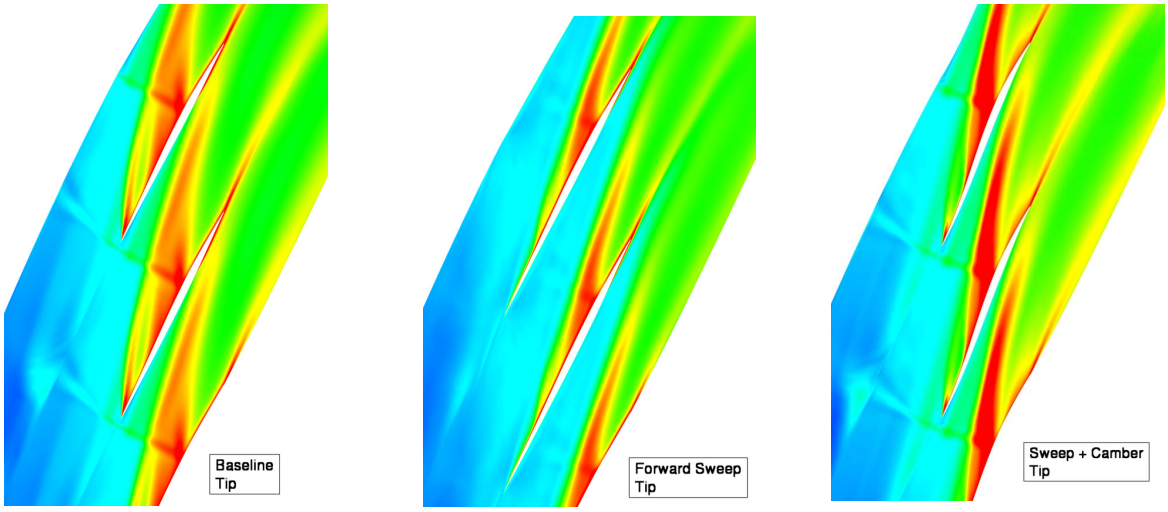

(a) Baseline Blade (b) 1st Optimization Blade (c) 2nd Optimization Blade

Fig9 Comparison of Entropy contours at 99% height section

The spanwise distribution of the axial velocity and adiabatic efficiency are presented in Fig.10. It shows that the axial velocity increases at the tip section due to the forward sweep and decreases below 50% span. This is the consequence of a spanwise redistribution of loading. In combination with the reduced shock strength and the smaller leakage flow, it results in a considerable gain in the adiabatic efficiency in the tip region with only a slight decrease in the hub region. These mechanisms are quite consistent with previous observations [7,8] and therefore verify the validity of present optimization system.

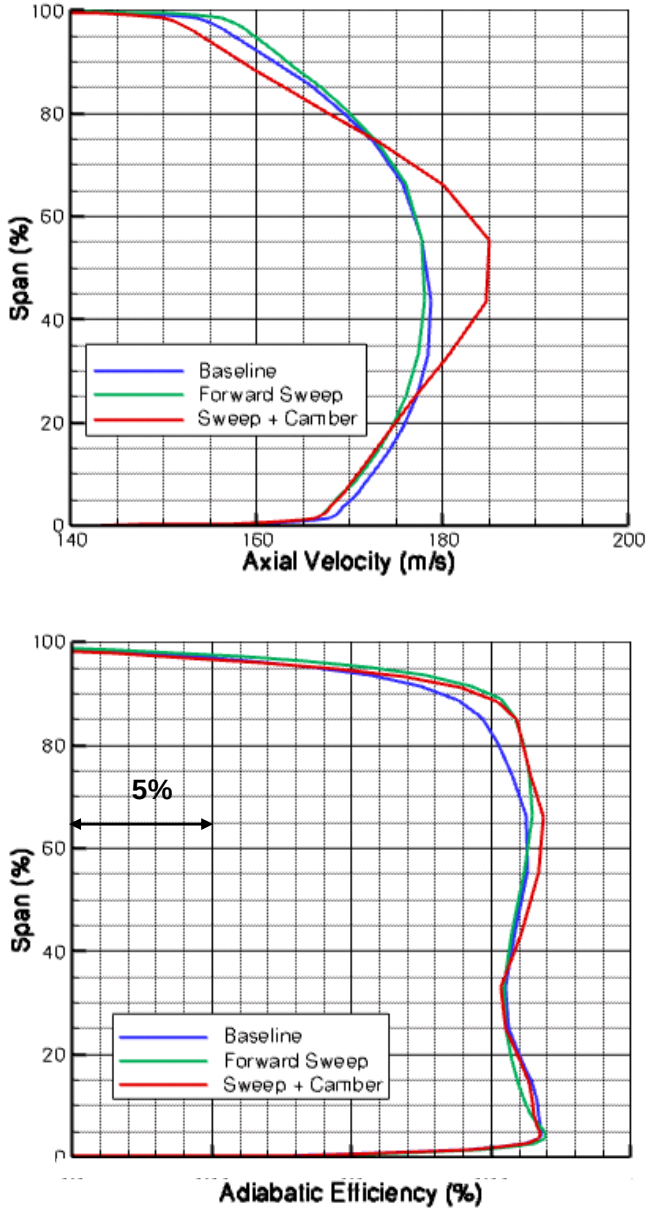

Fig.10 Axial velocity and efficiency distributions

The second optimization allows a modification of the camber line in addition to sweep and chord length. Figure 11 shows that the optimized geometry has a relatively strong backward sweep and a slightly barreling chord, which helps to reduce the mid-span loading and weakens the shock.

Figure 12.a shows a comparison between the camber lines at 90% height. It is noted that the optimized blade has an S-shaped camber line with negative camber in the front chord area and the peak camber position moved 18% upstream. This position roughly corresponds to the throat which is just upstream of the location where the passage shock usually occurs.

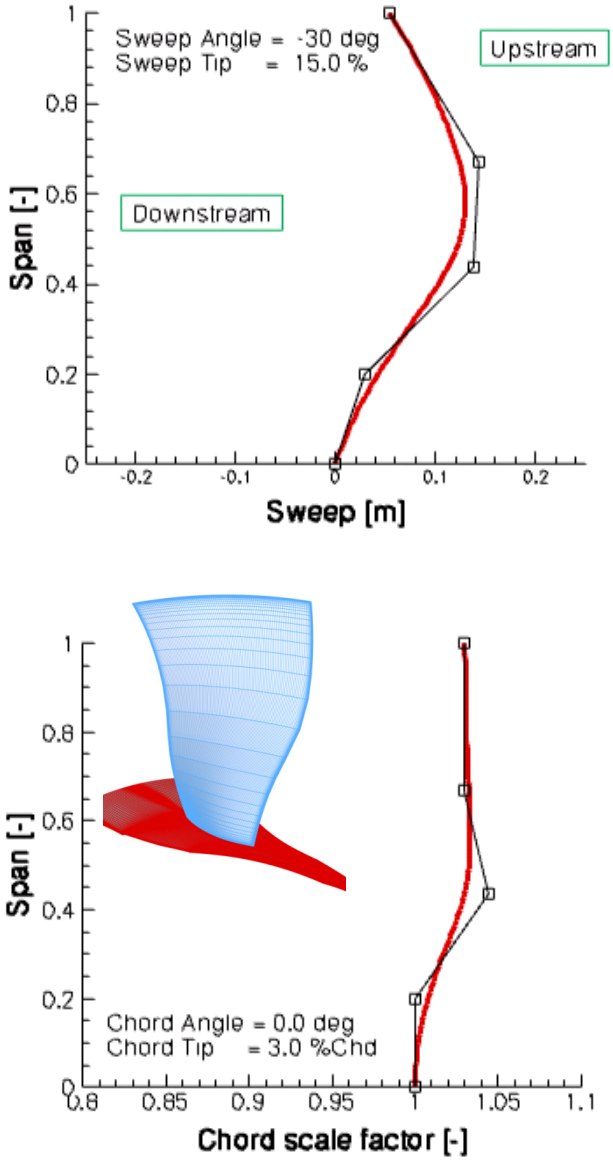

Fig.11 Resultant Geometry of the second optimization

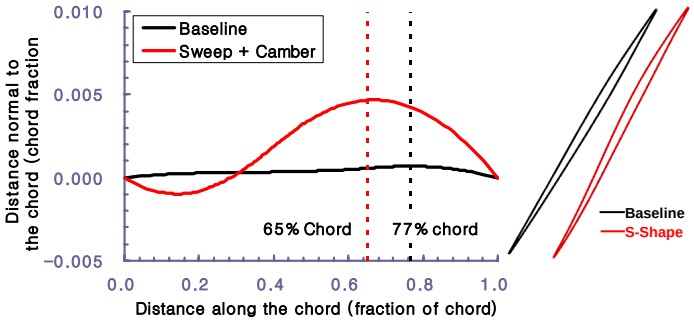

Fig.12.a Chordwise camber line distribution (90%Ht)

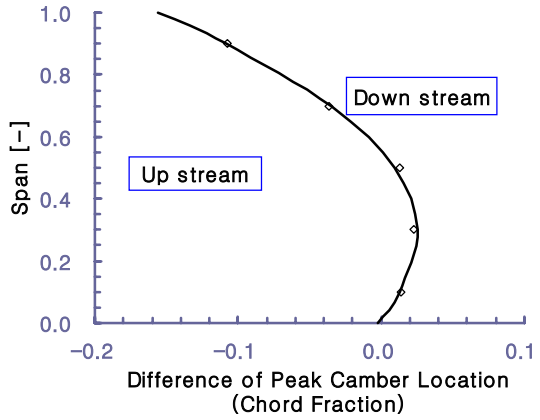

Fig.12.b Difference of peak camber Location

Figure 12.b shows the spanwise distribution of the shift in peak camber position between the baseline and the optimized blade. The corresponding forward shift in loading at the tip has the same effect as forward sweep.

The resulting performance map is shown in Fig.13. It includes the results of the first optimization for comparison. The 0.6% increase in the peak efficiency is considerably larger than in the previous optimization and sustained over the entire operation range. Moreover, the original stall margin is maintained in spite of the strong backward sweep.

Contrarily to the previous case, this blade is tip critical for the stability because of the backward sweep. However, a better global performance is obtained as confirmed from Fig.13, atttributed to the camber line control. This result verifies the conclusions that the optimum stacking distribution depends on the radial loading distribution of the baseline blade and that the present design system can find it and make a compromise between the performance and the stability

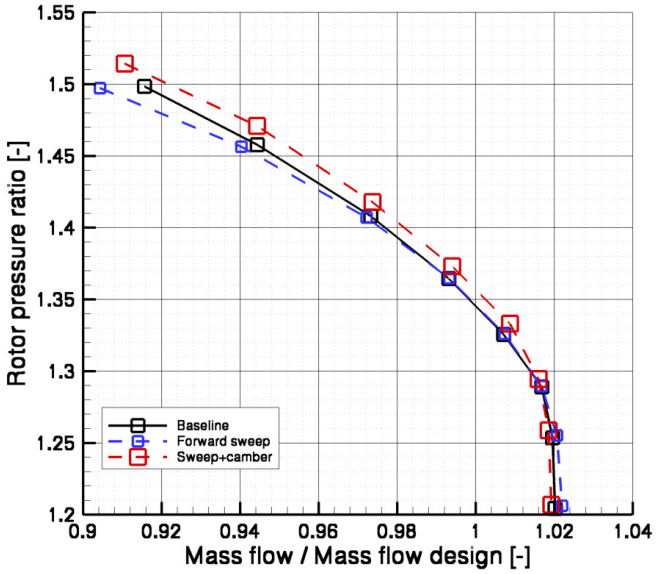

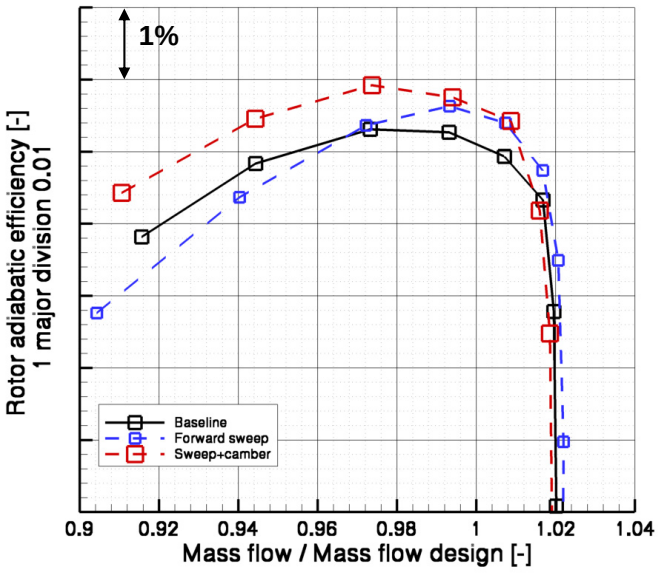

Fig.13 Compressor map

The tip Mach number distributions at the design operation point are superimposed on Fig. 14 to evaluate the camber-line effect. Figure14.a shows a comparison between the baseline blade and the second optimized one. The leading edge position of each blade is indicated by an arrow. It shows that the bow shock of the optimized blade is attached at the leading edge. In addition, the passage shock is more oblique in the blade to blade surface and is incident at the same point on the suction side as the baseline blade. This is the consequence of the forward sweep like effect introduced by the shift of maximum camber.

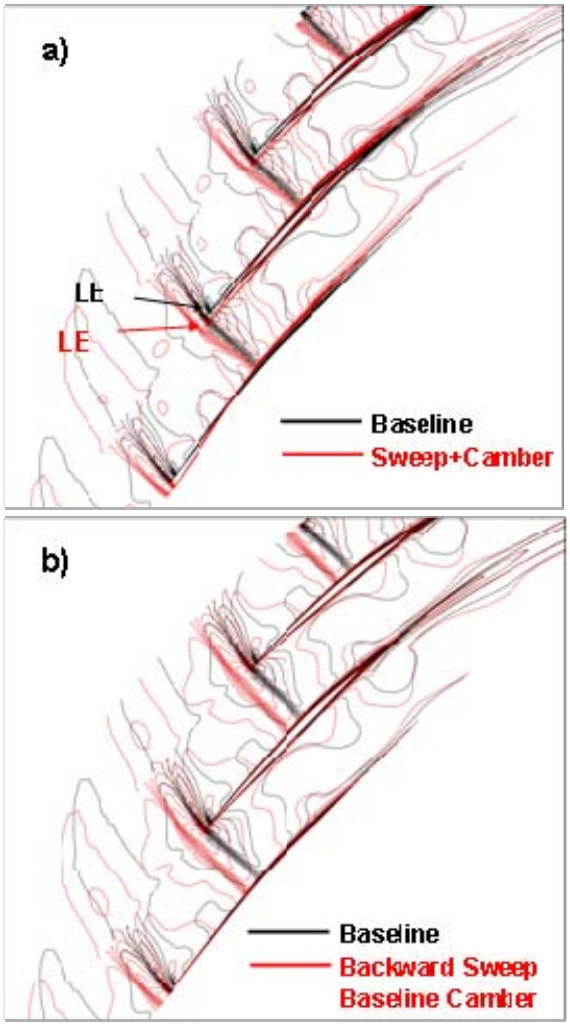

Fig.14 Superimposed tip Mach number contours

Figure 14.b is the comparison between the baseline blade and one with the optimized sweep and chord length but with the original camber line distribution. It shows that the bow shock is completely detached and normal to the suction side. This normal shock will move further upstream with increasing back pressure until stall occurs due to too high positive incidence. On the contrary, the oblique passage shock of the optimized blade will increase strength by increasing the shock angle and will remain attached to the leading edge. Therefore, the camber-line control stabilizes the blade by compensating for the shift of loading by the backward sweep.

Moreover the S-shaped profile at the tip section also improves the stability. As one can see from the pressure difference in the Fig.8.c it reduces the loading in the front part. The locally low loading in the front area at the tip section displaces the leakage flow to downstream (Fig.9.c). Hence the efficiency of the backward swept blade with the baseline camber starts decaying at 7% larger mass flow than the optimized one.

Another advantage of the S-shaped profile at the tip section is the smaller flow acceleration upstream of the bow shock (Fig. 8.c). It reduces the leading edge relative Mach number and results in a weaker shock. However the shock losses are higher than the equivalent subsonic diffusion losses. As a result, the loss at the tip section of the second optimization blade is also reduced in spite of the backward sweep (Fig.10). The backward swept blade with the original camber line did not show any efficiency improvement from the baseline one.

The meridional view of the static pressure contour is shown in Fig.7.c. The shock front is inclined at mid span due to the backward sweep and the extended chord locally reduces the peak Mach number. Consequently, the passage shock is significantly weakened and has partly disappeared in the mid span region. This is confirmed by the blade to blade static pressure contours on Fig. 8.f. Therefore, the mid span profits from the positive effect of the backward sweep without the disadvantages. Consequently, an efficiency gain is achieved over the entire span (Fig.10).

S-shaped profiles have a tendency to have a smaller throat section than cambered blades. However the local decrease of choking mass flow at the tip section is compensated by an considerable increase of the mass flow ad mid span (Fig. 10a). The axial velocity distribution, shown in Fig.10, indicate a relatively large radial loading shift of mass flow

The stage optimization.

Before carrying out this optimization, stage calculations have been made with the rotor geometries obtained by the previous optimizations. Figure 15 shows the different stage performance maps together with the full stage optimization results, explained later. The two optimized blades still demonstrate an advantage and the stall margins are consistent with the rotor only results. However the efficiency gain

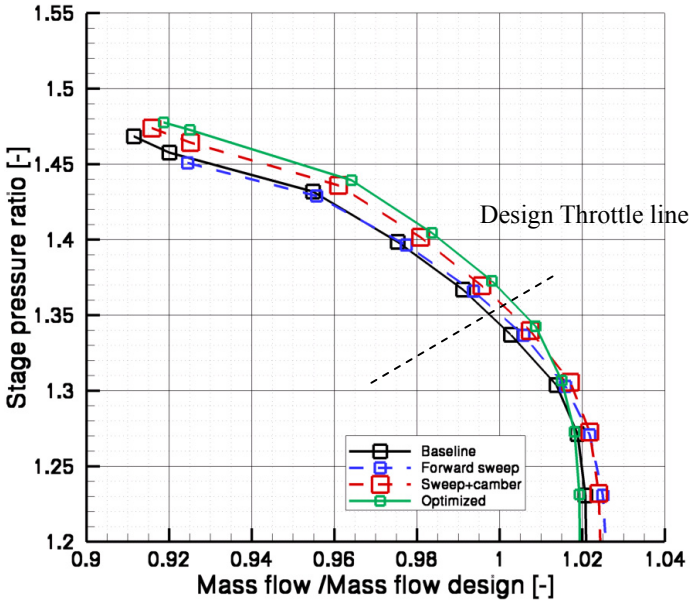

Fig.15.a Compressor map : Speed line

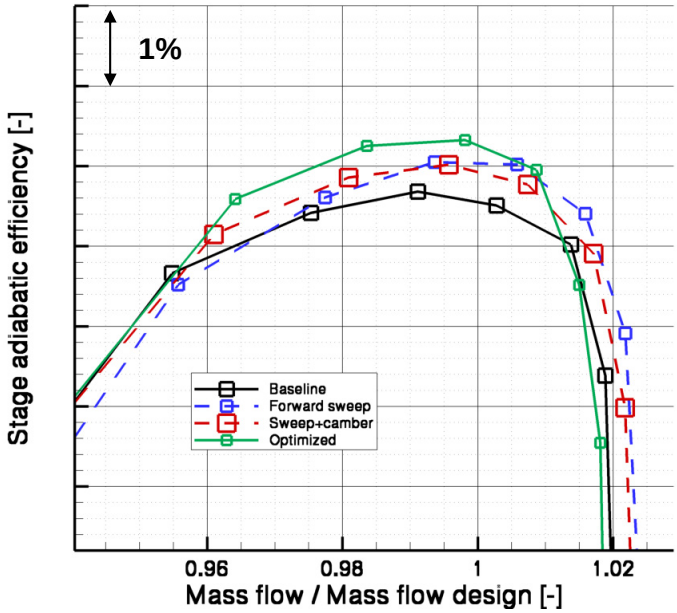

Fig.15.b Compressor map : Performance map

achieved in the 2nd single row optimization (backward swept blade) is reduced by 30% of its rotor only value.

Table 2 summarizes the performance change at the rotor peak efficiency point. It shows that the single row efficiency gain of the backward swept rotor is still the highest but that the stage efficiency is badly hurt by the increased stator losses.

Table.2 Performance at the Rotor peak efficiency point

	Opt.1	Opt.2
ΔRotor Efficiency	+0.37%.	+0.52%
ΔStage Efficiency	+0.37%	+0.18%
ΔStator Loss	+0.01%	+0.19%

(difference against the baseline blade case)

Figure 16 shows the absolute Mach number distribution at the stator inlet and exit. It is found that the backward sweep case has the highest inlet Mach number at the hub, which causes higher total pressure loss in this region. This rotor-stator interaction is responsible for the low gain in stage efficiency.

In order to avoid such a matching problem, the rotor geometry was optimized again, considering the full stage performance. Apart from a change of the rotor exit metal angle, the resulting geometry was almost equivalent to the S-shaped backward swept blade. However, the newly optimized blade showed a large (0.7%) improvement in stage efficiency while maintaining the stall margin (Fig.15).

Figure 17 shows the difference of the exit flow angle between the optimized blade and the baseline one. Positive values mean a decrease of the exit flow angle and thus, more turning. Although the exit flow angle is decreased over the entire span, it does not imply an increase of loading at the design point but a

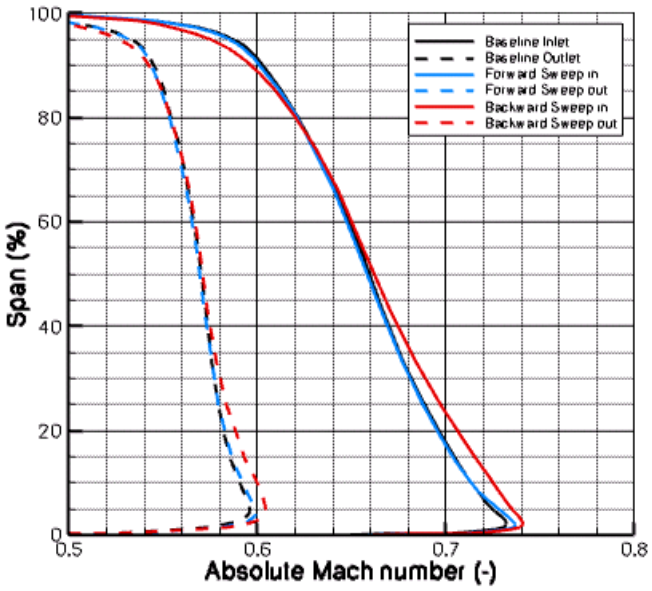

Fig.16 Stator inlet and outlet Mach number (Comparison of Single row optimization Geometries)

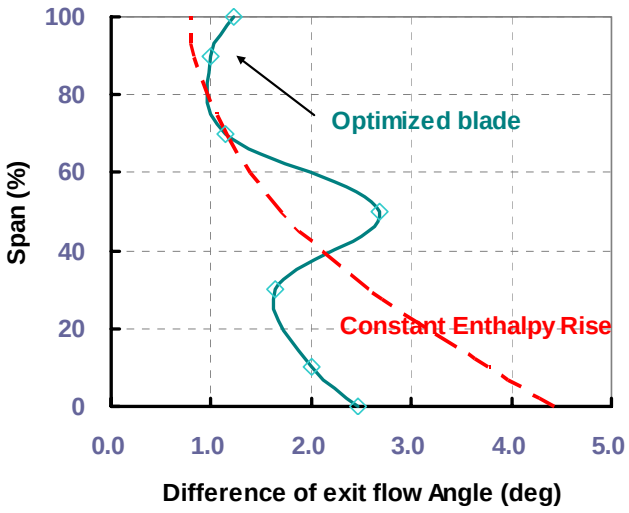

Fig.17 Difference of rotor exit flow angle

shift of the design point to a slightly higher mass flow point (see the design throttle line in figure 15.a).The design point is defined as constant throttle.

However, the change of exit angle modifies the spanwise loading distribution. For the comparison, Fig.17 includes the variation of outlet flow angle for a constant increase of enthalpy rise along the span, by which approximately the same decrease of the throttle from the design throttle value occurs. The difference between these curves characterizes the spanwise redistribution of the loading. It is found that the optimized

blade decreases the work at the hub relative to the mid and tip. It locally decreases the total pressure and hence the Mach number at the hub since the static pressure is established by radial equilibrium.

Figure 18 shows that the optimized blade indeed decreases the inlet Mach number at the hub, hence decreases the stator total pressure loss and improves the stage efficiency (Fig.15). Therefore, it can be considered that the camber-line control by the stage optimization compensates the negative effect of the backward sweep on the stage matching.

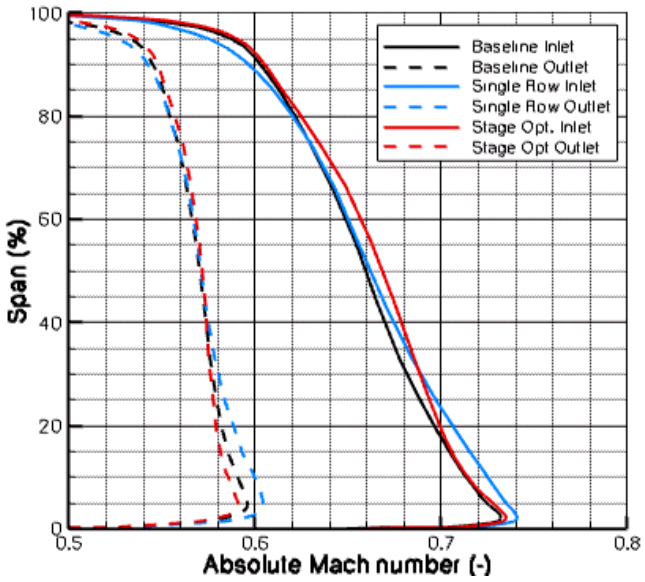

Fig.18 Stator inlet and outlet Mach number (Comparison of Single row and Stage optimization geometries)

In addition, since the pressure recovery in the tip area, is achieved by the combination of a shock wave followed by a subsonic diffusion, the reduction of the exit metal angle increases the rear camber and the extra subsonic diffusion further weakens the shock wave.

This is confirmed by the blade to blade static pressure contours at the tip of the stage optimized blade, compared in Fig.19 with the ones obtained by the single row optimization (2^{nd} case in stage operation). It appears that the bow shock became even more oblique.

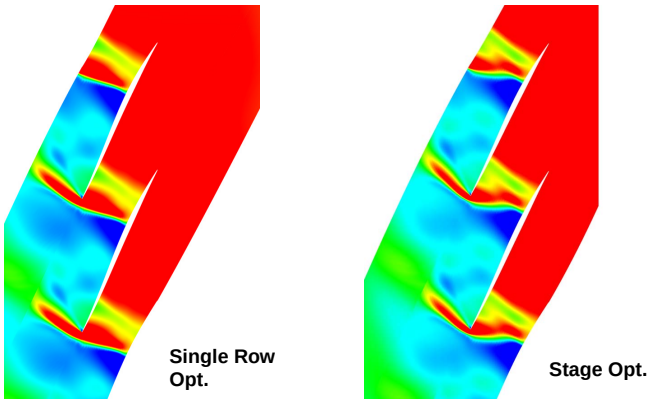

Fig.19 Static Pressure counters at 90% height

CONCLUSION

It has been shown that a three-dimensional optimization method is a powerful tool to find out what changes of the camber line, chord length and stacking distributions will result in performance improvements and to understand the mechanisms that govern the complex flow pattern in transonic compressors.

The following conclusions could be drawn.

1. The optimized geometry has a strong backward sweep stacking line, which together with a barreling chord length weakens the shock wave in the mid span region.
2. The optimum control of the camber line distribution makes the shock wave at the tip oblique in the blade to blade surface and attached at the leading edge similar to forward sweep. Therefore, it compensates the well-known negative effect of backward sweep on the stability and allows a 0.6% improvement in the rotor peak efficiency while maintaining the stall margin.
3. The stage calculation with the backward swept blade, obtained by the rotor only optimization, did not show the expected improvement in the stage efficiency because of the increased stator losses due to the strong radial loading shift induced by the backward sweep.
4 The latter can be avoided by a full stage optimization allowing also a change of rotor exit flow angle. The corresponding modification of the reaction reduced the stator loss and resulted in a 0.7% gain of stage efficiency at constant stall margin.

REFERENCES

[1] Prince, D. C., 1980, "Three-Dimensional Shock Structures for Transonic/Supersonic Compressor Rotors", AIAA journal of Aircraft Vol.17, pp28-37.

[2] Hah, C. and Wennerstrom, A.J., 1991, "Three-Dimensional Flow Fields Inside a Transonic Compressor with Swept Blades", ASME Journal of Turbomachinery Vol.113, pp.241-251.

[3] Yamaguchi, N., Tominaga, T. and Hattori,S., 1991, “Secondary-Loss Reduction by Forward-Skewing of Axial Compressor Rotor Blading”, International Gas Turbine Congress in Yokohama.

[4] Sasaki, T. and Breugelmans, F., 1997 “Comparison of Sweep and Dihedral Effects on Compressor Cascade Performance”, ASME Paper 97-GT-2.

[5] Law, C.H., and Wadia, A.R., 1993, “Low Aspect Ratio Transonic Rotors: Part1: Baseline Design and Performance”, ASME Journal of Turbomachinery Vol.115, pp.218-225.

[6] Law, C.H., and Wadia, A.R., 1993, “Low Aspect Ratio Trasonic Rotors: Part2: Influence of Location of Maximum Thickness on Transonic Compressor Performance”, ASME Journal of Turbomachinery Vol.115, pp.226-239.

[7] Wadia, A.R., Szucs, P.N. and Crall,D.W., 1998, “Inner Workings of Aerodynamics Sweep”, ASME Journal of Turbomachinery Vol.120 pp.671-682.

[8] Denton, J.D. and Xu, L., 2002, “The effects of Lean and Sweep on Transonic Fan Performance”, ASME GT2002-30327.

[9] Blaha, C., Kablitz, S., Hennecke, D.K., Schmidt-Eisenlohr,U., Pirker,K and Haselhoff,S., 2000, “Numerical Investigation of the Flow in an Aft-Swept Transonic Compressor Rotor”, ASME 2000-GT-0490.

[10] Beneini, E. and Biollo, R., 2006, “On the Aerodynanmics of Swept and Leaned Transonic Compressor Rotors” ASME GT2006-90547.

[11] Ji, L., Chen, J., and Lin, F., 2005, “Review and Understanding on Sweep in Axial Compressor Design”, ASME GT2005-68473.

[12] Medd, A.J., Dang, T.Q. and Larosiliere, L.M., 2003, “3D Inverse Design Loading Strategy for Transonic Axial Compressor Blading”, ASME GT2003-38501.

[13] Beneini, E., 2004, “Three-Dimesional Multi-Objective Design Optimization of a Transonic Compressor Rotor”, Journal of Propulsion and Power Vol.20 No.3, pp559-565.

[14] Watanabe,H. and Zangeneh,M., 2003, “Design of the Blade Geometry of Swept Transonic Fans by 3D Inverse Design”, ASME GT2003-38770.

[15] Demeulenaere, A. and Van den Braembussche, R.A., 1998, “Three-dimensional Inverse Method for Turbomachinery Blading design”, ASME Trans., Journal of Turbomachinery, Vol. 120, No. 2, April 1998, (pp. 247-255)

[16] Pierret, S., 1999, “Design Turbomachinery Blade by Means of the Function Approximation Concept Based on Artificial Neural Network, Genetic Algorithm and the Navier-Stokes Equations”, Von Karman Institute PhD. Thesis.

[17] Verstraete, T., 2008, “Multidisciplinary Turbomachinery Component Optimization Considering Performance, Stress and Internall Heat Transfer”, Von Karman Institute PhD. Thesis.

[18] Verstraete, T., Alsalihi, Z. and Van den Braembussche, R.A., 2007, “Multidisciplinary Optimization of a Radial Compressor for Micro Gas Turbine Applications”, ASME Journal of Turbomachinery, Vol.132, Issue 3, paper 021004.

[19] Amaral,S., Verstraete,T., Van den Braembussche,R.A., Arts,T., 2008, “Design and Optimization of the Internal Cooling Channels of a HP Turbine Blade Part1: Methodology”, ASME Journal of Turbomachinery, Vol.132, issue 3, Issue 3, paper 021013.

[20] Amaral,S., Verstraete,T., Van den Braembussche,R.A., Arts,T., 2008, “Design and Optimization of the Internal Cooling Channels of a HP Turbine Blade Part2: Optimization”, ASME Journal of Turbomachinery, Vol.132, Issue 3, paper 021014.

[21] Joly, M.; Verstraete, T.; Paniagua, G., 2010, “Attenuation of Vane Distortion in a Transonic Turbine using Optimization Strategies, Part I – Methodology” “Part II – Optimization”,
ASME Turbo Expo 2010: Power for Land, Sea and Air, Glasgow, United Kingdom, June 14-18, ASME GT2010-22370, ASME GT2010-22371

[22] Arnone, A., 1994, “Viscous Analysis of Three-Dimensional Rotor Flow Using a Multigrid Method”, ASME Journal of Turbomachinery Vol.116, pp.435-445.

[23] Sirakob, B. T. and Tan, C.S., 2002, “Effect of Upstream Unsteady Flow on Rotor Tip Leakage Flow”, ASME GT2002-358

[24] McNulty, G. S., Decker, J. J., Beacher, B. F. and Khalid, S. A., 2003, “The Impact of Forward Swept Rotors on Tip-Limited Low-Speed Axial Compressors”, ASME GT2003-38827.